JOURNAL OF GUIDANCE, CONTROL, AND DYNAMICS
Vol. 32, No. 1, January–February 2009

Cycler Trajectories in Planetary Moon Systems

Ryan P. Russell* and Nathan J. Strange†
Jet Propulsion Laboratory, California Institute of Technology, Pasadena, California 91109

DOI: 10.2514/1.36610

Free-return cycler trajectories repeatedly shuttle a spacecraft between two bodies using little or no fuel. Here, the cycler architecture is proposed as a complementary and alternative method for designing planetary moon tours. Previously applied enumerative cycler search and optimization techniques are generalized and specifically implemented in the Jovian and Saturnian moon systems. Overall, hundreds of ideal model ballistic cycler geometries are found and several representative cases are documented and discussed. Many of the ideal model solutions are found to remain ballistic in a zero radius sphere of influence patched conic ephemeris model, and preliminary work in a high-fidelity fully integrated model demonstrates near-ballistic cycles for several example cases. In the context of recent Cassini discoveries, the Saturn–Titan–Enceladus system is investigated in the most detail and many promising solutions result. Several of the high-energy Titan–Enceladus cyclers find immediate application as Cassini extended missions options that provide frequent low-altitude Enceladus flybys.

Nomenclature

a	=	semimajor axis
d	=	separation distance between orbiting body and primary
E	=	eccentric anomaly
e	=	eccentricity
f	=	short for full-revolution (even $n\pi$) transfer
g	=	short for generic (nonresonant) transfer
h	=	short for half-revolution (odd $n\pi$) transfer
M	=	integer number of flyby body full revolutions
N	=	integer number of spacecraft full revolutions
r	=	radius
r_P	=	periapse radius
T	=	period
t_p	=	time past periapse
v	=	velocity magnitude relative to primary
v_∞	=	velocity magnitude relative to flyby body
Z	=	scalar root-solving function
Δv	=	impulsive change to velocity magnitude
δ	=	turn angle for flyby
μ	=	gravitational parameter
ν	=	true anomaly

Subscripts

lb	=	lower bound
SOI	=	sphere of influence
TOF	=	time of flight
ub	=	upper bound

Introduction

CYCLER orbits offer a low propellant cost means for the exploration of multiple high-interest moons such as the Galilean moons at Jupiter, Titan, and the icy moons at Saturn. The Galilean moons have long been a top priority for space exploration. Europa, Ganymede, and Callisto each are speculated to support large subsurface liquid water oceans, and the proximity to the surface and the size of Europa's ocean has compelling astrobiological implications that make Europa the top priority of destinations on NASA's Solar System Exploration Roadmap‡ [1,2]. Io is extremely active volcanically and has a young surface, and Ganymede is the only moon in the solar system known to have a magnetic field [1]. At Saturn, Titan is one of the most Earth-like bodies in the solar system because of its complex atmosphere, methane hydrological cycle, dynamic surface, and organic signatures. Enceladus has recently become a high-priority target because Cassini identified ice crystal plumes that may originate from a liquid source extremely close to the surface [3,4].

Traditionally, cycler orbit theory has been applied to the sun–Earth–Mars system for ultimate application to human missions [5–19]. Earth–Mars cycler applications generally suffer from long repeat periods, infrequent launch opportunities, and the risky requirement to perform hyperbolic rendezvous [20]. In contrast, the brief synodic periods of most planetary moon pairs lead to an abundance of cycler solutions with short repeat periods and frequent initiation opportunities. Further, the mission objectives of a planetary moon cycler are achieved en route and during flybys only and therefore do not require hyperbolic rendezvous.

In this study, cycler search techniques previously applied to the Earth–Mars case are expanded to seek similar repeating trajectories between moons that orbit a common planet. The generalized cycler search algorithm provides timetables for the moon tour design space through an automated global search that finds and catalogs cycler opportunities. The cycler solutions identify feasible multibody flyby resonances useful as standalone designs or preliminary guesses for sequences of conventional planetary tour designs. The cycler trajectories can provide critical reconnaissance and communication for planned orbiters, surface landers, and aerial vehicles, whereas the repeat flybys enable remote sensing and in situ science of the multiple high-priority targets.

The first sections overview the existing cycler search and optimization algorithms, describe the improvements and generalizations, and discuss the relevant moon systems and dynamic models. Next, the automated ideal (circular–coplanar) model search is applied to find cyclers for four Jovian moon pairs and the

Presented as Paper AAS 07-118 at the AAS/AIAA Space Flight Mechanics Meeting, Sedona, AZ, 29 January–1 February 2007; received 11 January 2008; revision received 16 May 2008; accepted for publication 19 May 2008.

*Engineer, 4800 Oak Grove Drive; currently Assistant Professor, School of Aerospace Engineering, Georgia Institute of Technology, 270 Ferst Drive, Atlanta, Georgia 30332-0150; ryan.russell@gatech.edu. Member AIAA.

†Senior Engineer, 4800 Oak Grove Drive, Mail Stop 301-165; nathan.strange@jpl.nasa.gov. Member AIAA.

‡http://solarsystem.nasa.gov/multimedia/downloads/SSE_RoadMap_2006_Report_FC-A_med.pdf [cited 11-30-06].

Titan–Enceladus pair in the Saturn system. Special attention is paid to Titan and Enceladus because Cassini discoveries have recently thrust both moons into the science spotlight. Each ideal model search results in hundreds of ballistic solutions. The solutions and characteristics are archived and a select few of the best cases are documented and discussed. Several of the solutions are optimized over multiple periods in a zero radius sphere of influence patched conic ephemeris model and remain ballistic. Of the most promising solutions is the Titan–Enceladus cycler #235 that includes nine targeted Enceladus encounters, 45 targeted Titan encounters, full-orbit rotation around Saturn (for complete lighting conditions), and near Hohmann velocities at Enceladus during a 2.4 year flight time. Several of the higher-energy Titan–Enceladus cyclers have potential applications for Cassini extended missions. Finally, to demonstrate the transition from the patched conic ephemeris model to a high-fidelity model, multiple legs of a select few cyclers are optimized in a fully integrated n-body plus oblateness model.

Approach

The general cycler trajectory problem is to find an indefinitely repeatable pattern of ballistic trajectories that cycle a spacecraft between two celestial bodies that orbit a common body. The repeatability requirement makes the problem substantially more difficult than typical intermoon or interplanetary spacecraft tours. In general, exactly repeatable cyclers only exist in simplified models. Therefore, the approach for solving the general cycler problem is reduced to two steps:

1) Perform a broad search for true cyclers in an ideal model consisting of circular and coplanar celestial body orbits. These ideal model cyclers are exactly periodic.

2) Evaluate and optimize multiple cycles of ideal model cyclers in more realistic models. Because the geometry of the realistic solar system model is not exactly periodic, each cycle of a realistic cycler will be quasi periodic. In this study, two levels of fidelity are considered for realistic models: a) zero radius sphere of influence patched conic ephemeris model, and b) fully integrated n-body plus oblateness model.

To reduce the search space to a manageable size, a subset of cyclers called *free-return cyclers* are sought, in which one of the two orbiting celestial bodies in the ideal model is considered massless. This assumption is removed when considering the higher-fidelity noncircular and noncoplanar models. Note that [18] is a recent cycler study that presents an elegant method allowing gravity-assisted flybys at both bodies in the ideal model cycler problem. Currently, we restrict the ideal model problem to be free-return cyclers only. For the case of the Sun–Earth–Mars system, the free-return cyclers in ideal and more realistic models are computed and analyzed in detail in [5–18]. The current study generalizes the methods outlined in [11,13] to find free-return cyclers between any two celestial bodies that orbit a common body with near-circular, near-coplanar orbits. A brief overview of the method follows.

First, two bodies of interest are identified that have near-circular, near-coplanar orbits around a common body. Next, the magnitude of the spacecraft hyperbolic excess velocity v_∞ with respect to the flyby body is chosen. Assuming the ideal circular–coplanar model, all direct free-return trajectories are calculated with the specified v_∞ that leave the flyby body and return ballistically within a specified maximum flight time. This procedure is described in detail in [10]. The solutions are easily visualized as a set of points and lines on the v_∞ globe, as the example in Fig. 1 illustrates. The vertical arrow represents the body velocity vector, and the v_∞ globe is the locus of the tips of all possible v_∞ vectors that emanate from the tip of the body velocity vector. The z direction is aligned with the body velocity, and the x direction is aligned with the body position with respect to the primary, leaving the y direction to be orthogonal to the body orbit plane.

In Fig. 1, solutions that return to the body after exactly an integer number of body revolutions around the primary exist as circles on the surface of the globe and are labeled "full-rev circles." These types of free returns are commonly referred to as resonant transfers. Solutions that return to the body after exactly an even integer number of half-body revolutions around the primary exist as points on the surface of the globe. They appear as above- and below-orbit plane pairs and are labeled "half-rev 'x's" and "half-rev 'o's," respectively. Lastly, all free-return solutions with transfer angles that are not integer numbers of half-body revolutions exist as single points labeled "generic dots" and are constrained to the spacecraft orbit plane.

Gravity-assisted flybys provide a mechanism to connect multiple free-return trajectories. The flyby has the effect of rotating an incoming v_∞ vector by an angle whose magnitude is a function of the flyby altitude and the flyby body mass. In the circular–coplanar model, the incoming and outgoing v_∞ magnitudes for all free-return trajectories are always identical. Therefore, a tour of free-return trajectories patched by gravity-assisted flybys can be constructed as discrete steps on the v_∞ globe, where each step represents a rotation of the v_∞ vector. The maximum size of each step is limited by the turn angle associated with a flyby of a specified minimum altitude. The free-return cycler problem is then reduced to a combinatorics problem of finding repeatable patterns that step the v_∞ vector from free-return solution to free-return solution. More specifically, we want to find all 1-leg, 2-leg, ..., n-leg patterns that require valid flybys to navigate the v_∞ vector around the v_∞ globe on free-return solutions, with a

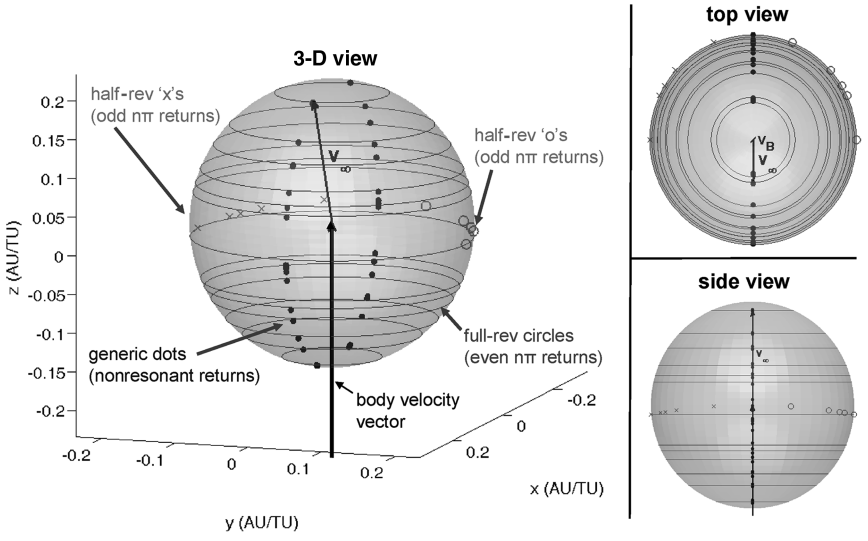

Fig. 1 Example v_∞ globe identifying all three types of possible free-return solutions: half-revolution (odd $n\pi$ transfer angle), full-revolution (even $n\pi$), and generic (non-$n\pi$).

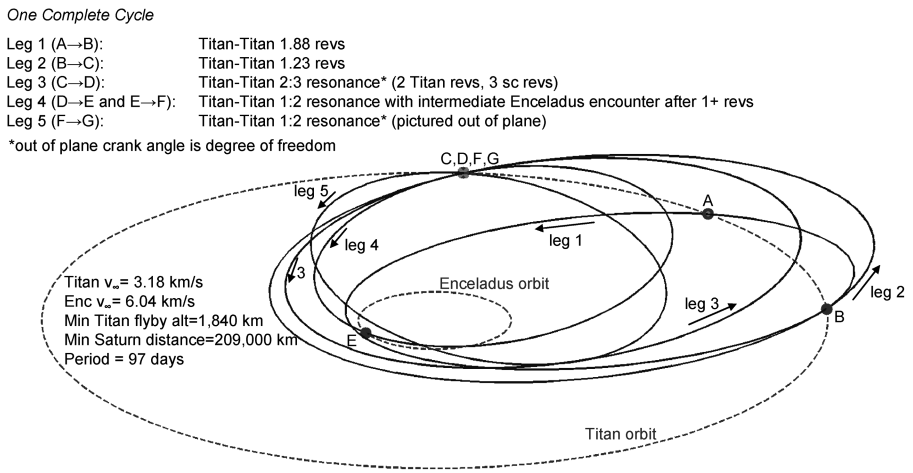

Fig. 2 Three-dimensional diagram of one cycle of the ideal model Titan–Enceladus cycler #235.

total combined flight time that is an integer multiple of the synodic period of the two bodies of interest. If at least one of the free-return solutions includes a trajectory that crosses the path of the second body of interest, then the pattern can be initiated such that an encounter occurs every period. Enumerating all of the possible combinations of half-revolution, full-revolution, and generic returns is well documented in [11]. The process is repeated for a full range of v_∞ values and results in a list of exactly periodic cyclers in the ideal model with a variety of defining characteristics.

For evaluation in a more realistic model, the ideal model solutions are propagated for several repeat cycles in the ideal model and a homotopy (i.e., a continuation) method is employed to parametrically walk the solution to a zero radius patched conic model that considers ephemeris locations of the bodies and models flybys as instantaneous body-centered velocity rotations. A final trajectory of up to ~50 legs is sought that is ballistic in the patched conic ephemeris model. This highly constrained trajectory optimization problem is described in detail in [13].

Finally, the resulting solutions are used as initial guesses for optimization in a high-fidelity force model, including integrated flybys, n-body perturbations, and central-body oblateness. The high-fidelity optimization is performed with Mystic, a general-use software tool under development at the Jet Propulsion Laboratory [21]. Improving strategies for transitioning from the low- to the high-fidelity ephemeris solutions is an ongoing topic of research and warrants detailed future study. Here, it is emphasized that the high-fidelity optimization is included only to demonstrate reasonable Δv costs associated with realistic planetary moon cyclers.

Figure 2 illustrates an example of a cycler trajectory. A complete cycle is shown in detail of one of the most promising ideal model cyclers found in this study. The cycler begins at Titan on the 'A' label and performs a free return to 'B' after 1.88 revs. A gravity-assist flyby places the cycler on a 1.23 rev free return to 'C' and is followed by a 2:3 and consecutive 1:2 resonant returns to complete the cycle. The targeted Enceladus encounter occurs at 'E' in the middle of the fourth leg or the first 1:2 resonant free return. Each gravity-assisted flyby at Titan, including the flyby required to patch consecutive cycles, is well above the minimum altitude of 1000 km (the lowest flyby is 1843 km), making the cycler ballistic in the ideal model.

Improved Cycler Search Capabilities

The search and optimization techniques from [11,13] are generalized to deal robustly with the vastly different time and distance scales associated with interplanetary and intermoon cyclers, including the ability for the flyby body to be inside or outside the orbit of the target body. The following subsections highlight the most important capabilities enabled by the current study.

Nonresonant Free-Return Calculation

Given a specified v_∞, direction of motion (direct or retrograde), $M_{\max}$ where M is the floor of the number of flyby body revolutions, an algorithm is sought that provides all existing nonresonant return trajectories (or generic dots from Fig. 1). The approach from [10] is based on a computationally expensive table lookup method, whereas the new approach relies on a one-dimensional root-solving procedure and requires less memory storage and computational effort [22]. Note that [18] also presents an graphical semi-analytic method for obtaining nonresonant return orbits that are feasible candidates for inclusion in cycler orbits.

Figure 3 shows the period vs flight time and v_∞ for all direct nonresonant free returns to a body in a circular orbit with $M \leq 3$ calculated from the multiple revolution Lambert problem [23–25]. It is emphasized that both the long and short period direct solutions from the classical Lagrange formulation of the Lambert problem [23,24] are reported in Fig. 3. However, the inbound vs outbound specification indicates the sign of the initial flight-path angle and is unrelated to the short vs long period specification. The objective is to obtain an algorithm that finds all intersections of a horizontal line of constant v_∞ with the solution curves from the lower half of Fig. 3 (for arbitrary v_∞ and $M_{\max}$).

Algorithm 1 reduces the problem to a one-dimensional root-solving problem that requires iteration on the period T of the transfer ellipse. Note that all equations are normalized such that the circular radius of the flyby body is one length unit (LU) and the gravitational parameter of the primary is unity. Direct solutions are possible for v_∞ values between zero and $\sqrt{3}$, while retrograde solutions are possible for v_∞ values between 1 and $1 + \sqrt{2}$.

Algorithm 1 initially calculates the minimum transfer semimajor axis $a_{\min}$ from the conic equation, and the minimum period follows. The maximum transfer flight time $\mathrm{TOF}_{\max}$ is calculated, noting that one normalized flyby body period is 2π time units (TU). For a given M, the maximum floor of the number of transfer revolutions $N_{\max}$ is calculated, assuming the smallest possible transfer period and the largest possible flight time. For a given M and N, lower and upper bounds on the transfer period guess are derived from inspection and expressed as T_{lb} and T_{ub}, respectively.[§] Next, T is iterated to seek solutions to the equation $Z = 0$, for both inbound and outbound transfers. If a solution exists, then $T_{\mathrm{lb}} < T < T_{\mathrm{ub}}$.

The highly nonlinear equation for Z is calculated as follows. Equations (1) and (2) give the transfer semimajor axis and departure velocity from two-body dynamics:

$$a = [T/(2\pi)]^{2/3} \tag{1}$$

[§]The upper bound of infinity results only in the retrograde $N = 0$ case due to the possibility of the near parabolic solution. To avoid the infinite bound, a max eccentricity (i.e., 0.99) can be enforced and a max period can be found by solving Eq. (3), which reduces to a cubic in terms of T.

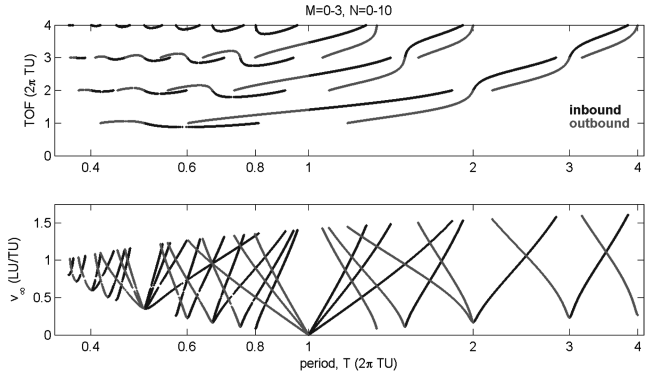

Fig. 3 All direct nonresonant free returns to a body in circular orbit for $M \leq 3$.

$$v = \sqrt{2 - 1/a} \tag{2}$$

Equation (3) then provides the transfer eccentricity as a function of v_∞. This expression is related to Tisserand's condition, and details of the derivation are found in [22]:

$$e = \sqrt{1 - (v^2 + 1 - v_\infty^2)^2/(4a)} \tag{3}$$

Equation (4) gives the absolute value of the departure true anomaly from the conic equation, and Eq. (5) expresses this as eccentric anomaly:

$$\nu = |\cos^{-1}[(a - ae^2 - 1)/e]| \tag{4}$$

$$E = \tan^{-1}[2\tan(\nu/2)\sqrt{(1-e)/(1+e)}] \tag{5}$$

The short time to periapse is then

$$t_p = [E - e\sin(e)]/(2\pi/T) \tag{6}$$

Finally, $Z(M, N, v_\infty, \text{inout}, \text{direction})$ is expressed in Eq. (7) as the difference between the flight times of the spacecraft and the flyby body. For further details, see [22]:

$$Z = \begin{cases} [TN + 2t_p] - [2\pi M + 2\nu] & \text{IF inout=inbound, direction=direct} \\ [T(N+1) - 2t_p] - [2\pi(M+1) - 2\nu] & \text{IF inout=outbound, direction=direct} \\ [TN + 2t_p] - [2\pi(M+1) - 2\nu] & \text{IF inout=inbound, direction=retrograde} \\ [T(N+1) - 2t_p] - [2\pi M + 2\nu] & \text{IF inout=outbound, direction=retrograde} \end{cases} \tag{7}$$

Over the valid range of $T_{\text{lb}} < T < T_{\text{ub}}$, Z is imaginary in some regions and suffers from multiple sign changes in the first and second derivatives with respect to T. One solution method for solving $Z(T) = 0$ is to march through the valid range of T and initiate a gradient based root-solver when Z is real and a sign change is detected. Note that a few rare cases are observed where Z has two roots for fixed M, N, direction, and inout. (See the double valued v_∞ in Fig. 4.) However, from observation, the double valued solutions are near the impractical eccentricity of 1. An example application of the algorithm finds 220 nonresonant direct free returns with $v_\infty = 0.5$ LU/TU when considering $M \leq 9$.

For the case of Titan as the flyby body, all nonresonant retrograde transfers with $v_\infty < 1.5$ LU/TU have periapse smaller than the radius of the outermost obstructive rings at 2.92 Saturn radii. If the resonant inclined orbits are considered, a few nonimpact retrograde orbits begin to exist for $v_\infty > 1.12$ LU/TU. Note that the end of mission Cassini v_∞ is expected to be ~1.1 LU/TU. It is therefore not restrictive to ignore retrograde solutions for a cycler Cassini extended mission. Although it is possible to construct cyclers with retrograde orbits, it is generally not beneficial because the large v_∞ values reduce the available flyby bending angles and thus require prohibitively long cycle repeat periods. Despite its impracticality for the current application, Algorithm 1 applies to retrograde as well as direct solutions.

Transitioning Ideal Model Solutions to a Patched Conic Ephemeris Model

An improved approach for the homotopy method is implemented to parametrically "walk" an ideal model solution into a multiple-cycle solution in a more realistic model. A previous approach [13] relies on the mean orbital elements of the orbiting celestial bodies, in which successive subproblems are solved by slowly increasing the eccentricities and inclinations from circular–coplanar values to the true values, and the last subproblem is solved using ephemeris body locations. The technique works well in the case of planets such as Earth and Mars, where reality is closely modeled by Keplerian motion. However, the method struggles in the case of planetary moons, where perturbations from other moons and central-body oblateness cause the motion to be poorly predicted using mean orbital elements.

The new approach parametrically walks the solution from the patched conic ideal model to a patched conic ephemeris model using several subproblems, where the locations of the orbiting bodies are determined by a linear interpolation between the ideal model and ephemeris locations. Thus, for successive subproblems, the model slowly morphs from a circular–coplanar model into an ephemeris model. The approach is robust and easy to implement because it does not rely on user-supplied mean elements for either body.

Models

The generalized free-return cycler search is applied to each of the ideal model systems in Table 1, where the primary is considered inertially fixed and the flyby and target bodies are in circular–coplanar orbits around the primary.

All four Galilean moons of the Jovian system are of high science interest and are capable of enabling significant gravity-assisted flybys. Although the target body in the idealized model is assumed to be massless, a free-return cycler connecting two massive bodies is possible as long as the flyby altitudes at the target body are sufficiently high. Although the higher flyby altitudes may be less desirable in terms of science, the extra degree of freedom enabled by the inclusion of target-body flybys will prove useful when transitioning to more realistic models. The four Jovian cycler systems investigated are representative of the body pairs of highest scientific interest. Europa and Io are perhaps the most scientifically attractive bodies, however Jupiter's radiation environment prohibits long spacecraft exposure in their vicinities. Ganymede is the largest

Algorithm 1 For calculating all nonresonant returns with a specified v_∞ and maximum flight time

IF $v_\infty \geq 1 + \sqrt{2}$, THEN "no elliptical solution exists" STOP
$v_{\min}^2 = (1 - v_\infty)^2$
$a_{\min} = 1/(2 - v_{\min}^2)$
$T_{\min} = 2\pi\sqrt{a_{\min}^3}$
FOR $M = 0, M_{\max}$
  $\text{TOF}_{\max} = 2\pi(M + 1)$
  $N_{\max} = \text{int}(\text{TOF}_{\max}/T_{\min})$
  FOR $N = 0, N_{\max}$
    $T_{\text{lb}} = \max[T_{\min}, 2\pi M/(N + 1)]$
    $T_{\text{ub}} = \text{TOF}_{\max}/\max(N, 1)$
    IF ($N = 0$ & direction = retrograde), THEN
      IF ($v_\infty \geq \sqrt{2} - 1$), THEN $T_{\text{ub}} = \infty$
      ELSE
        $T_{\text{ub}} = 2\pi(1 - v_\infty^2 - 2v_\infty)^{-3/2}$
    inout = {inbound, outbound}
    FOR EACH inout
      Root solve $Z(v_\infty, M, N, \text{inout, direction}, T) = 0$, where $T_{\text{lb}} < T < T_{\text{ub}}$ if solution(s) exist
      IF (successful), THEN record solution properties
    END inout
  END N
END M

body and experiences relatively benign radiation in comparison to the closer moons. Therefore, Ganymede is chosen as the flyby body for cyclers to each of the other moons. To improve the frequency and altitudes of the Europa encounters, a Europa–Ganymede cycler is also considered. Note, the Ganymede–Callisto cyclers will experience the least radiation dose of all the Jovian cyclers.

The Saturn–Titan–Enceladus system is perhaps the best planetary moon application for the free-return cycler theory because both moons are of high science priority and the assumptions of the idealized model are exceptionally accurate. The Titan and Enceladus orbits are nearly circular and coplanar, and Titan is capable of providing the gravity-assists as it is the largest moon in the Saturn system by almost 2 orders of magnitude. Furthermore, the small mass of Enceladus validates the massless assumption of the target body in the ideal model, thus enabling arbitrarily low flyby altitudes and excellent opportunities for science. Figure 5 illustrates how the hyperbolas at Enceladus are effectively straight lines, as the mass is insufficient to significantly bend the trajectories. Low-altitude flybys are therefore possible with any B-plane angle as a degree of freedom. The opportunities to begin a cycler reoccur frequently because the synodic period of Titan and Enceladus is a very brief 1.5 days.

Table 1 Planetary moon ideal models considered

Primary	Free-return flyby body	Target body
Jupiter	Ganymede	Io
Jupiter	Ganymede	Europa
Jupiter	Ganymede	Callisto
Jupiter	Europa	Ganymede
Saturn	Titan	Enceladus

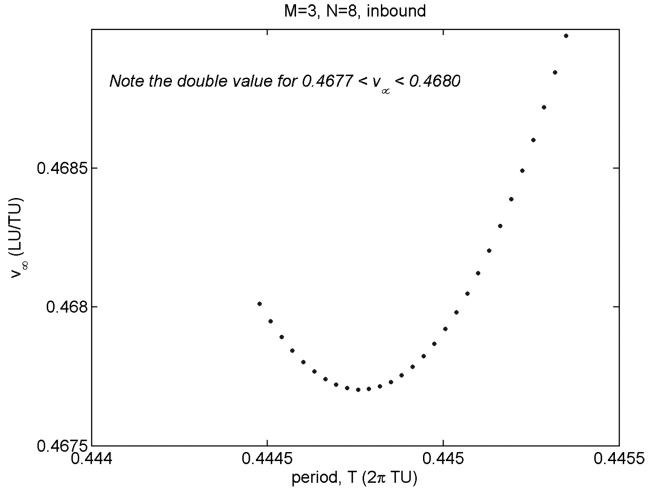

Fig. 4 Zoomed view of Fig. 3.

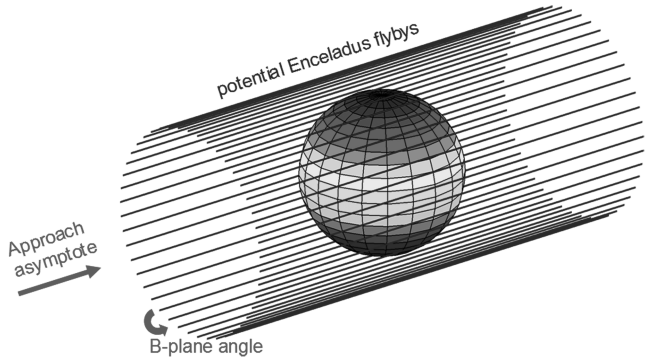

Fig. 5 Flyby geometry at Enceladus.

In addition to the Jovian and Saturnian cyclers, several heliocentric cyclers were investigated to test and calibrate the general capability of the improved methods to work across different time and distance scales. The heliocentric ideal models considered were the Earth–Mars, Earth–Venus, Venus–Mars, and Venus–Mercury systems. A few of the resulting previously undocumented heliocentric cyclers are recorded in [26]. However, for space considerations, only planetary moon cyclers are presently considered.

Table 2 reports the parameters for each relevant body. It is emphasized that the gravitational parameter of the target body (for example Enceladus in the Saturn–Titan–Enceladus system) is not required for the ideal model free-return cycler search. However, the gravity of the target body *is* considered when transitioning ideal model solutions to more realistic models. The patched conic ephemeris model optimization relies strictly on ephemeris files[¶] for body locations and is independent of mean orbital elements. The inclinations and eccentricities are reported in Table 2 only to indicate the validity of the circular–coplanar assumptions of the idealized

[¶]http://naif.jpl.nasa.gov/naif/spiceconcept.html [cited 15 December 2006]; ftp://naif.jpl.nasa.gov/pub/naif/generic_kernels/spk/planets/de414.bsp [cited 15 December 2006]; ftp://naif.jpl.nasa.gov/pub/naif/generic_kernels/spk/satellites/jup230.bsp [cited 15 December 2006]; ftp://naif.jpl.nasa.gov/pub/naif/generic_kernels/spk/satellites/a_old_versions/sat242.bsp [cited 15 December 2006].

Table 2 Body parameters

Body	Gravitational parameter, $\mu(km^3/s^2)$	Radius, km	Ideal model circular orbit period, s	Ephemeris model mean eccentricity[a]	Ephemeris model mean inclination[a], deg
Jupiter	126,686,535	71,492	Primary	Primary	Primary
Saturn	37,931,208	60,268	Primary	Primary	Primary
Io	5959.92	1827	152,854	0.0041	0.036
Europa	3202.74	1561	306,822	0.0094	0.469
Ganymede	9887.83	2634	618,153	0.0011	0.170
Callisto	7179.29	2408	1,441,931	0.0074	0.187
Titan	8978.14	2575	1,377,684	0.0288	0.280
Enceladus	6.95	256.3	118,387	0.0047	0.009

[a]http://ssd.jpl.nasa.gov [cited 15 Dec. 2006].

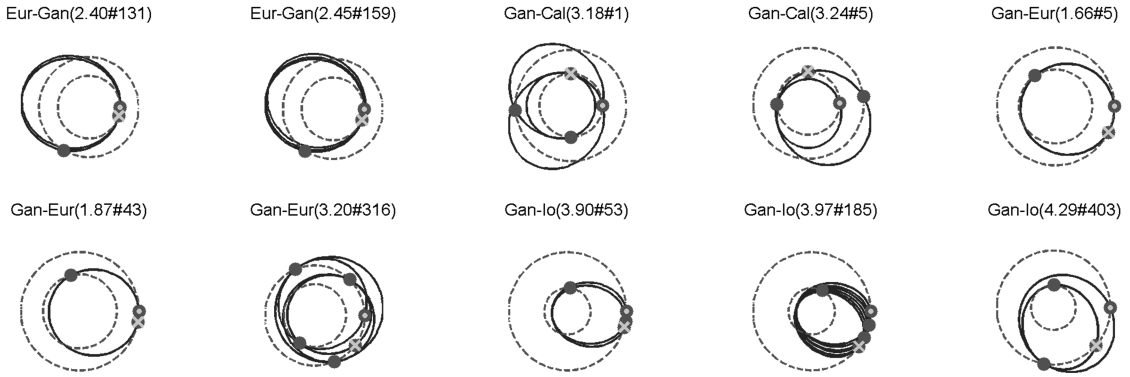

Fig. 6 Representative Jovian ideal model ballistic cyclers.

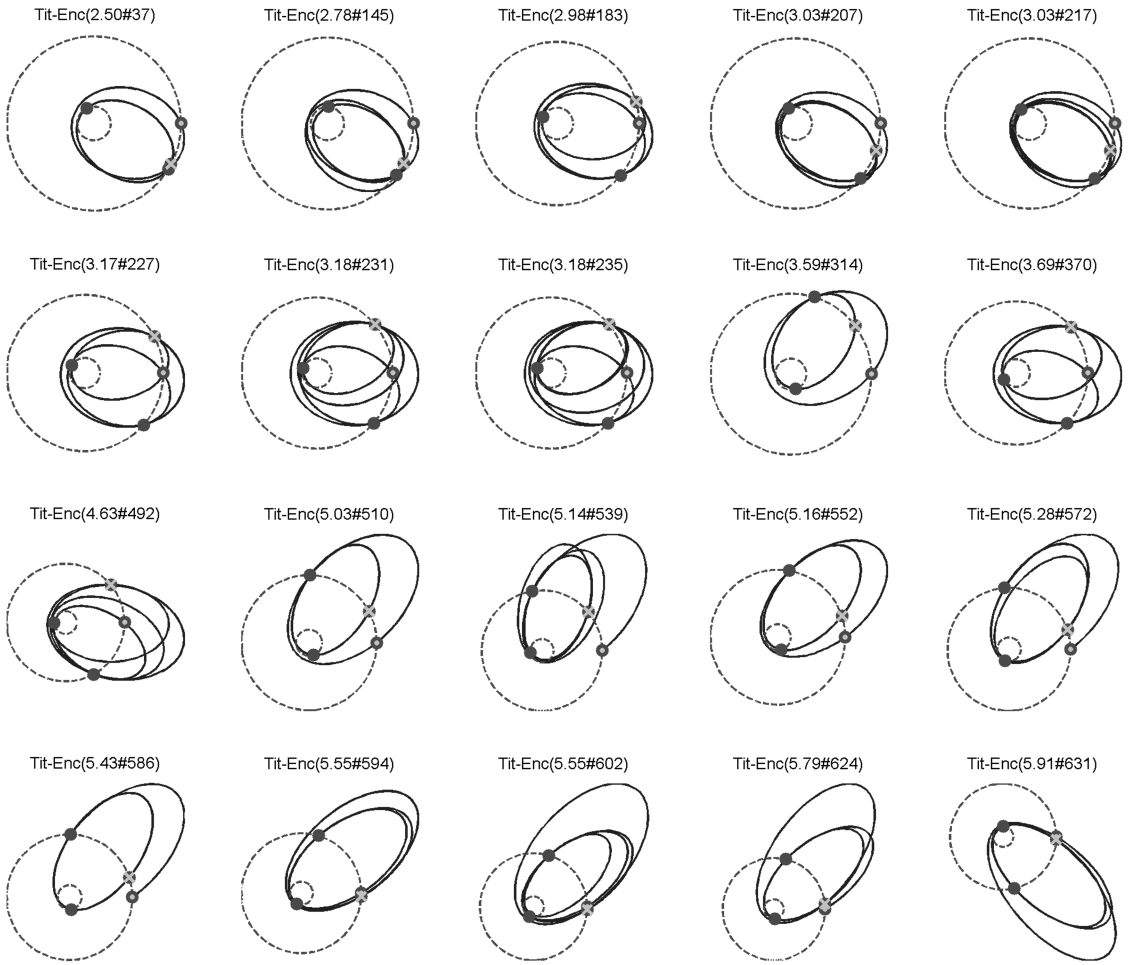

Fig. 7 Representative Titan–Enceladus ideal model ballistic cyclers.

Table 3 Characteristics of promising Jovian ballistic ideal model cyclers

Body A	Body B	ID	Synodic period, day	v_∞ A, km/s	v_∞ B, km/s	Number of legs	Period, day	Petal period, yr	Min flyby alt. at body A, km	Min dist. to primary, km	Max dist. to primary, km	Transit A → B, day	Transit B → A, day
Europa	Ganymede	131	7.05	2.40	4.10	2	21.2	−1.33	1113	669,299	1,459,266	5.65	8.40
Europa	Ganymede	159	7.05	2.45	4.11	3	28.2	−1.33	1261	667,983	1,459,994	5.63	8.37
Ganymede	Callisto	1	12.52	3.18	3.26	3	37.6	0.41	247	826,589	2,415,871	9.90	2.61
Ganymede	Callisto	5	12.52	3.24	3.34	2	37.6	0.41	328	821,915	2,390,844	10.14	16.67
Ganymede	Europa	5	7.05	1.66	2.57	1	35.3	−1.33	1819	633,307	1,080,067	12.14	23.11
Ganymede	Europa	43	7.05	1.87	3.89	1	14.1	−1.33	8861	564,558	1,072,330	6.52	7.58
Ganymede	Europa	316	7.05	3.20	3.81	4	49.4	−1.33	1447	592,969	1,496,829	7.60	12.23
Ganymede	Io	53	2.35	3.90	9.85	2	21.2	−1.33	518	280,283	1,075,918	8.65	5.54
Ganymede	Io	185	2.35	3.97	9.90	6	49.4	−1.33	603	277,384	1,080,403	8.62	5.50
Ganymede	Io	403	2.35	4.29	4.34	2	56.4	−1.33	540	412,959	1,336,522	17.14	12.63

models. Although the mean eccentricities and inclinations of the planetary moons are generally low, it is emphasized that the n-body perturbations and the oblateness effects of the primary are revealed in nontrivial perturbations to the osculating Keplerian orbital elements.

All patched conic flybys referred to in this study are modeled with the assumption that they occur instantaneously and the radius of the flyby body's sphere of influence is zero. The instantaneous change in the flyby body centric velocity direction is given by Eq. (8):

$$\sin\left(\frac{\delta}{2}\right) = \left(\frac{\mu}{\mu + r_p v_\infty^2}\right) \tag{8}$$

Note that other more realistic (and complicated) patched conic models exist, such as those that include hyperbolic conic propagation and sphere of influence patch point locations.

Finally, the highest-fidelity force models considered include full numeric integration of the equations of motion without resorting to patched conics. The example Titan–Enceladus cyclers include Saturn oblateness and point mass gravity for the Saturnian moons with gravitational parameters larger than 1 km^3/s^2. The example Ganymede–Europa cycler includes Jupiter oblateness and point mass gravity for each of the Galilean moons. The ephemeris locations of the bodies are found from the same ephemeris files that are used for the patched conic model.[¶] The poles and prime meridians for Jupiter and Saturn are based on the most recent data from the International Astronomical Union Working Group on Cartographic Coordinates and Rotational Elements of the Planets and Satellites [27]. A point mass sun is also considered in the high-fidelity model.

Idealized Model Cycler Search

Each ideal model cycler search results in hundreds of variations of cyclers with a variety of defining characteristics. Although the solution sets are too large to document here, the complete trajectories are archived for future use. A sampling of previously undocumented promising ideal model cyclers is summarized in the following figures and tables. Figures 6 and 7 illustrate the trajectories for full cycles of selected promising solutions, where each cycle begins on the dot and ends on the cross, and the numbers in the parenthesis of each title indicate the flyby body v_∞ in kilometers per second and the solution identification, respectively.

Tables 3 and 4 report important metrics that characterize and define each free-return cycler solution illustrated in Figs. 6 and 7. The short synodic periods of the planetary moon systems lead to a large number of solutions, and the multiple timing variations of each solution lead to a vast design trade space when comparing solutions for different applications. The following paragraphs discuss the important cycler characteristics and design trades associated with each of the columns of Tables 3 and 4.

The v_∞ values at the flyby body and the target body are important measures of energy. Depending on the source of the cycler spacecraft, the cost of initiating a cycler can increase or decrease with v_∞. The initiation cost for an Earth–Mars cycler increases with Earth v_∞ because the cycler must be initially launched from Earth [9]. On the other hand, a planetary moon cycler will often be more expensive to initiate for lower values of flyby body v_∞ because the cycler spacecraft initiates from an interplanetary trajectory ending in a high-speed hyperbolic approach.

To insert into a planetocentric cycler from an interplanetary trajectory, propulsive (or perhaps aerocapture) maneuvers are required to capture around the planet and ultimately achieve the correct moon-centered v_∞. The rendezvous cost from the cycler to the flyby or target body scales directly with v_∞. Science measurements during a flyby of either body will be directly impacted by the body-centered velocities. Depending on the instruments and applications, it may be desirable to perform flybys with both large and small v_∞ values.

The "number of legs" column in Tables 3 and 4 indicates the number of flyby body free-return trajectories, in which one of the legs includes an encounter with the target body. Thus, a cycler with n legs

Table 4 Characteristics of promising ballistic Titan–Enceladus ballistic ideal model cyclers

ID	v_∞ Tit., km/s	v_∞ Enc., km/s	Number of legs	Period, day	Petal period, yr	Min flyby alt. at Tit., km	Min dist.[a] to Saturn, km	Max dist. to Saturn, km	Transit Tit. → Enc., day	Transit Enc. → Tit., day
37	2.50	5.17	2	94.4	−3.34	1377	219,772	1,296,179	39.85	40.04
145	2.78	7.33	3	94.4	−3.34	1067	185,227	1,335,036	31.94	32.23
183	2.98	4.66	3	64.5	4.16	3304	227,827	1,441,656	10.65	5.29
207	3.03	5.08	4	63.0	−3.34	3905	192,449	1,372,495	10.60	5.34
217	3.03	5.08	4	63.0	−3.34	10,059	192,449	1,372,495	5.17	10.78
227	3.17	5.98	3	80.9	2.90	1183	209,397	1,555,251	10.50	5.45
231	3.18	6.04	4	97.4	2.41	2140	208,590	1,637,907	10.49	5.46
235	3.18	6.04	5	97.4	2.41	1843	208,590	1,637,907	10.49	5.46
314	3.59	6.88	2	49.5	1.32	1218	196,276	1,673,806	19.52	10.77
370	3.69	4.15	3	97.4	2.41	1343	221,429	1,798,164	21.54	26.30
492	4.63	5.61	4	97.4	2.41	4085	220,423	2,494,396	14.67	14.49
510	5.03	7.27	2	80.9	2.90	1852	196,399	2,531,474	15.81	29.31
539	5.14	8.08	4	97.4	2.41	1821	183,032	2,898,708	29.36	15.84
552	5.16	7.69	2	112.4	6.06	3784	189,939	2,431,736	30.66	30.39
572	5.28	4.69	3	112.4	6.06	1798	201,896	2,899,479	56.37	19.99
586	5.43	6.68	2	112.4	6.06	3874	208,262	2,899,438	73.04	19.50
594	5.55	5.76	3	127.4	−38.20	6348	210,686	2,944,806	22.31	22.14
602	5.55	5.76	4	127.4	−38.20	1469	168,068	3,563,396	22.31	22.14
624	5.79	7.97	3	95.9	15.77	1961	189,020	3,606,073	22.49	22.23
631	5.91	7.49	3	127.4	−38.20	4243	197,913	3,625,914	21.66	45.42

[a]For the Titan–Enceladus cyclers, Saturn's G rings pose a hazard out to $r \sim 176,000$ km. Synodic period = 1.50 days.

has $n + 1$ flybys per cycle. For science purposes, it is desirable for a cycler to include as many flybys as possible.

The cycler period is the combined time of flight (TOF) of each leg and is constrained to be an integer multiple of the system synodic period. Because there is only one guaranteed encounter with the target body per full cycle, the cycler period dictates the frequency of target-body encounters. As [11] illustrates, the number of cycler solutions increases dramatically as the allowable period increases. Furthermore, the enumerating technique becomes practically infeasible when the allowable cycler periods are too long. For reasonable computation run times (less than a few days on one modern processor), a general rule of thumb is to seek solutions with periods less than or equal to eight flyby body periods. This rule limits the number of potential cycler legs to approximately 10. Less exhaustive searches, such as the one described in [9], can substantially increase the number of potential legs and the cycler period, however, these solutions do not include $n\pi$ transfers when $n > 2$. To emphasize the importance of short delays between successive target-body encounters, the enumerating technique based on [11] is used exclusively for the present study.

The petal periods reported in Tables 3 and 4 are a measure of the angular difference in locations of the flyby body between consecutive cycles. If the trajectories are considered "petals" on a flower that is centered at the primary, the petal period is the time required to complete the flower with 2π radians of petals. This metric is most important for the planetocentric cyclers with flyby bodies that are synchronously locked with their orbital rates. For the synchronously rotating body, the sequence of $v_{\infty-}$ and $v_{\infty+}$ vectors associated with each flyby remains unchanged in the body-fixed frame for successive periods. (The only exception is the case of a resonant flyby where there is a potential degree of freedom in choosing the placement of v_∞ along the full-rev circle, as illustrated in Fig. 1.) Therefore, in the idealized model, the ground tracks of each flyby of the gravity-assist body will be identical for successive cycles. For example, if there are four flybys of the gravity-assist body during each cycle, then the set of the four ground tracks will be repeated every cycle (again, with the exception of any resonant flybys with a degree of freedom). Of course, when perturbations of a realistic model are considered, the ground tracks are expected to be quasi periodic rather than exactly repeating as in the ideal model.

Because the periods of the planetocentric cyclers are short compared with the orbital period of the primary, the sun-line direction is approximately fixed. Consequently, the lighting conditions for science measurements during each flyby will change as the orientation of the petals rotate around the primary. The petal period is therefore the approximate time required to achieve all possible lighting conditions for each of the $n + 1$ flybys on a given cycler. For the planetocentric cyclers with synchronously rotating bodies, a short petal period is highly desirable. Note that the sign of the petal period indicates the direction of rotation.

The minimum and maximum distances to the primary may be useful for filtering cyclers that exceed a desired range of operation. The Saturn-centric cyclers require a conservative minimum distance of 2.92 Saturn radii ($\sim$176, 000 km) to avoid harmful ring particle collisions.

The final two columns of Tables 3 and 4 report the transit times involving the target body. As mentioned previously, each ideal model cycler consisting of free-return trajectories to the flyby body can be initiated at multiple times such that an encounter with the target body is ensured. The transit leg trajectory will intersect the path of the target body once on an inbound path and once on an outbound path (except in the limiting case where the periapse of the transit is the radius of the target-body orbit). Further, the inbound- and outbound-encounter opportunities are repeated for each revolution of a multiple revolution transit leg. It is emphasized that multiple pairs of transit times are possible for each cycler reported in Tables 3 and 4, although only one pair is listed. For operational purposes, it is difficult to schedule consecutive flybys within 3 or 4 days (and transit times greater than 10 days are preferable). For the fast-moving systems such as the Titan–Enceladus system, a minimum transit time of 3 days is an important constraint because many of the favorable cycler solutions fail to have any transit time pairs that meet this requirement. Note that transit time pairs with near equal magnitudes will generally lead to improved convergence properties when transitioning the solution to an ephemeris model.

Tables 5 and 6 provide the formal nomenclature associated with each of the reported ideal model cyclers. The purpose of the naming system is to provide an efficient means of describing these complicated trajectories uniquely. Given the definitions outlined in [12] and a descriptor string for each leg of an arbitrary cycler, all of its characteristics can be calculated, and the entire trajectory can be systematically reproduced. Note that each leg begins with an h, f, or g representing a half-revolution (odd $n\pi$), full-revolution (even $n\pi$), or a generic (non-$n\pi$) free return, respectively. A capital letter indicates the leg that includes the target-body encounter.

Patched Conic Ephemeris Model Optimization

Multiple cycles of a few example cyclers are transitioned to the patched conic ephemeris model and illustrated in Figs. 8–12.

Table 5 Formal nomenclature for cyclers from Table 3

ID	Leg 1	Leg 2	Leg 3	Leg 4	Leg 5	Leg 6
EurGan#131	G(3.95655, 704.35739, U)	f(2:1, 87.95239, 90.00000)	——	——	——	——
EurGan#159	G(3.94206, 699.14318, U)	f(2:1, 87.24509, 120.26932)	f(2:1, 87.24509, 59.73068)	——	——	——
GanCal#1	G(1.74871, 269.53421, U)	g(1.50246, 540.88534, L)	f(2:1, 77.40130, 0.03291)	——	——	——
GanCal#5	g(1.50425, 541.53130, L)	G(3.74691, 628.88825, U)	——	——	——	——
GanEur#5	G(4.92758, 2493.92898, U)	——	——	——	——	——
GanEur#43	G(1.97103, 1069.57159, U)	——	——	——	——	——
GanEur#316	g(1.31322, 472.76044, U)	h(1.5, 540.0, L, −3.98557)	g(1.31322, 472.76044, U)	G(2.77217, 1357.97970, U)	——	——
GanIo#53	g(0.97232, 710.03419, U)	G(1.98423, 1434.32320, U)	——	——	——	——
GanIo#185	g(0.96288, 706.63724, U)	f(1:2, 84.97911, 89.99999)	g(0.96288, 706.63724, U)	f(1:2, 84.97911, 57.73932)	G(1.97285, 1430.22609, U)	f(1:2, 84.97911, 90.00890)
GanIo#403	g(3.72334, 1700.40403, Ll)	G(4.16078, 2217.88234, L)	——	——	——	——

Table 6 Formal nomenclature for cyclers from Table 4

ID	Leg 1	Leg 2	Leg 3	Leg 4	Leg 5
TitEnc#37	g(0.91247, 688.48877, U)	G(5.01017, 3963.66276, L)	——	——	——
TitEnc#145	g(0.89794, 683.25735, U)	G(4.02471, 3248.89419, L)	f(1:2, 64.90258, 142.00153)	——	——
TitEnc#183	g(0.89055, 680.59930, U)	g(2.15189, 1134.67873, U)	F(1:2, 61.35060, 180.0)	——	——
TitEnc#207	g(0.88869, 679.92726, U)	g(1.05974, 741.50710, Ll)	F(1:2, 60.31038, 180.0)	f(1:2, 60.31038, 167.71581)	——
TitEnc#217	g(0.88869, 679.92726, U)	F(1:2, 60.31038, 0.0)	g(1.05974, 741.50710, Ll)	f(1:2, 60.31038, −179.90781)	——
TitEnc#227	g(0.88489, 678.56001, U)	g(3.19166, 1508.99845, U)	F(1:2, 57.91040, 180.0)	——	——
TitEnc#231	g(0.88468, 678.48383, U)	g(1.22599, 441.35506, U)	f(3:5, 55.34820, 167.71581)	F(1:2, 57.76202, 180.0)	——
TitEnc#235	g(0.88468, 678.48383, U)	g(1.22599, 441.35506, U)	f(2:3, 55.18988, 179.99996)	F(1:2, 57.76202, 180.0)	f(1:2, 57.76202, 154.65857)
TitEnc#314	g(1.20284, 433.02184, U)	G(1.89950, 1403.81944, Ls)	——	——	——
TitEnc#370	g(0.87690, 675.68567, Ls)	g(2.23376, 804.15321, U)	F(3:5, 48.53243, 180.0)	——	——
TitEnc#492	G(1.82913, 1018.48816, L)	f(1:1, 40.91079, 0.00006)	g(2.28153, 461.35072, U)	f(1:1, 40.91079, 179.99987)	——
TitEnc#510	g(2.24732, 449.03519, U)	G(2.82923, 1378.52326, L)	——	——	——
TitEnc#539	g(1.27588, 99.31575, U)	f(1:1, 35.08563, 179.99992)	G(2.83479, 1380.52313, L)	f(1:1, 35.08563, −0.00001)	——
TitEnc#552	g(3.22220, 799.99089, U)	G(3.82857, 1738.28475, L)	——	——	——
TitEnc#572	g(1.26162, 94.18203, U)	G(4.78915, 1724.09360, L)	f(1:1, 33.41047, −0.00438)	——	——
TitEnc#586	g(1.24728, 89.02223, U)	G(5.80348, 2089.25340, L)	——	——	——
TitEnc#594	g(2.20335, 433.20509, U)	G(2.78752, 1003.50729, L)	f(3:2, 34.01307, 0.00040)	——	——
TitEnc#602	g(2.20335, 433.20509, U)	f(1:1, 30.24411, −176.67648)	G(2.78752, 1003.50729, L)	f(2:1, 36.04284, 0.00001)	——
TitEnc#624	g(1.21211, 76.36107, U)	G(2.80454, 1009.63414, L)	f(2:1, 33.39447, −0.01457)	——	——
TitEnc#631	g(1.78380, 642.16785, L)	G(4.20707, 794.54453, U)	f(2:1, 32.10391, 179.99994)	——	——

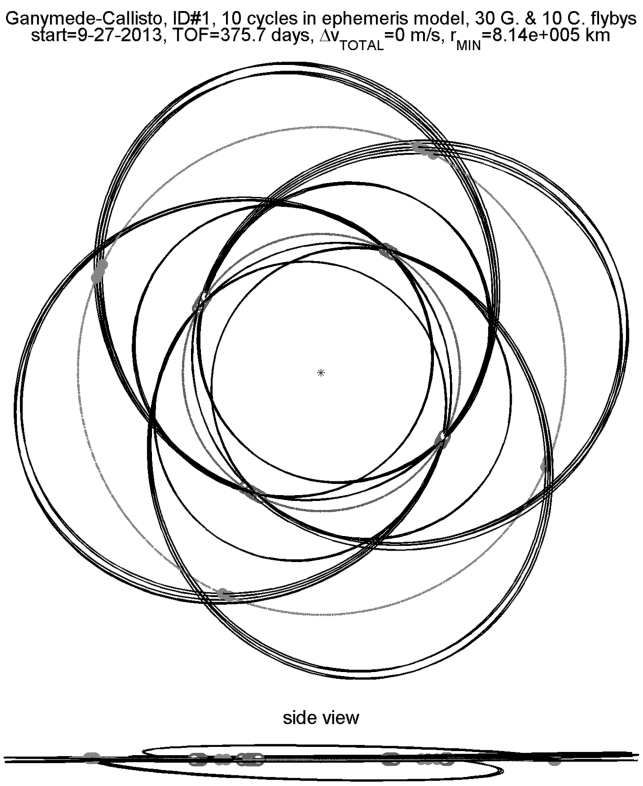

Fig. 8 Example Ganymede–Callisto ephemeris patched conic cycler.

Remarkably, many of the cyclers remain ballistic. The Ganymede–Callisto #1 solution from Fig. 8 is a representative ballistic solution that enjoys very low radiation exposures and an extremely short petal period (~0.41 years from Table 3), as indicated by the completion of ~2.5 rotations around Jupiter over the course of 10 cycles. The Ganymede–Europa #316 ballistic solution from Fig. 9a is noteworthy because of its many legs, the large out-of-plane motion, and the inclusion of a 3π transfer ** (second leg from Table 5). The Europa–Ganymede #131 solution from Fig. 9b is a relatively simple cycler that enables two Europa flybys and one Ganymede flyby every 21 days, and the radiation exposure is minimized because it never goes inside Europa's orbit.

Figures 10–12 give examples of Titan–Enceladus patched conic ephemeris cyclers. Of the low v_∞ solutions, #235 from Fig. 11b is particularly promising. This example includes 45 Titan flybys, 9 Enceladus flybys, and a flight time of 2.4 years. The Enceladus encounters are equally spaced around Saturn, enabling the full possibilities of lighting conditions, and the trajectory easily converges to ballistic due to the large flyby altitudes in the ideal model solution. Furthermore, as is common for all planetary cyclers, initiation opportunities are abundant because of the short synodic period (1.5 days for Titan–Enceladus system).

Note that all the free-return cyclers are guaranteed to have exactly one target-body encounter per cycle. However, the fast Enceladus period leads to the possibility for many untargeted flybys, especially when the transit leg includes multiple revolutions. Close inspection of the cycler #235 in Fig. 11b shows 24 additional encounters with close approaches less than 200,000 km, while four of those are less than 100,000 km. As a second example, the transit leg on the #37 cycler from Fig. 10a is an 11+ revolution transfer. Thus, in addition to the eight targeted Enceladus flybys, there are 17 untargeted Enceladus flybys with close approaches less than 100,000 km, where nine of those are less than 25,000 km. The frequency and proximity of the untargeted flybys are highly sensitive to a specific epoch.

**The odd-$n\pi$ solutions are sought in all of the ideal model cycler searches in this study. However, unlike the Earth–Mars case [11], ballistic solutions that include odd-$n\pi$ free returns are much less common for the planet-centered cyclers considered.

Table 7 gives the pertinent data for the example patched conic ephemeris model cycler #235 shown in Fig. 11b. Although the Titan–Enceladus system is circular–coplanar to first order, a quick comparison between the times and v_∞ values of Tables 4 and 7 illustrates the nontrivial effects of using an ephemeris vs a circular–coplanar model.

The v_∞ at Titan for the Cassini spacecraft has spanned the approximate range of $5.8 \rightarrow 6.0$ km/s. Considering that small v-infinity leveraging maneuvers [22] can significantly reduce flyby body v_∞, the ideal model Titan–Enceladus cyclers with $v_\infty >$ ~5 km/s (see Table 4) are reasonable for extended mission (and extended-extended mission) consideration. Of the high-energy cyclers, those in Fig. 12 are illustrated because of their short petal periods leading to favorable rotation rates around Saturn. The out-of-plane component of solution #572 from Fig. 12a is also attractive; however, as the title indicates, this 562 day trajectory requires 222 m/s Δv and fails to remain outside of Saturn's G ring radius of 176,000 km. The #586 trajectory from Fig. 12b remains outside the G ring and requires 154 m/s to achieve 5 Enceladus and 10 Titan encounters in 561 days. Because the higher v_∞ trajectories are dynamically more constrained, the patched conic ephemeris optimization outlined in [13] converges to ballistic solutions much easier for trajectories with low v_∞. Noting that the method in [13] has only a limited ability to minimize Δv for nonballistic trajectories, it is anticipated that detailed optimization of any one trajectory with a high-fidelity optimizer will reduce Δv requirements. As a low-energy example, note that cycler #314 from Table 4 is attractive because of short repeat time, short petal period, and favorable timing; however, in the ephemeris case, we observe that ballistic solutions were not readily found and a more sophisticated optimization would likely improve the results.

High-Fidelity Optimization

The assumptions of the zero radius sphere of influence patched conic ephemeris model include several nontrivial error sources that manifest when transitioning solutions to a high-fidelity model. These error sources include the nonzero radius of the sphere of influence, central-body oblateness, and n-body perturbations. For the examples considered in this study, the largest of these error sources is the assumption that the sphere of influence for the flyby body is negligible compared with the size of the flyby orbit around the primary. A common definition for the radius of the sphere of influence around a small body in a circular orbit around a primary is given in Eq. (9), where d is the separation distance between the bodies [28]:

$$r_{\mathrm{SOI}} = d(\mu/\mu_{\mathrm{primary}})^{2/5} \tag{9}$$

The patched conic assumption is clearly better in the case of the heliocentric cyclers, noting that $r_{\mathrm{SOI}} \sim 0.006d$ for the sun–Earth system compared with $\sim 0.035d$ for the Saturn–Titan system, $\sim 0.023d$ for the Jupiter–Ganymede system, and $\sim 0.014d$ for the Jupiter–Europa system. Furthermore, the oblateness effects of the primary and n-body perturbations (both of which are ignored in our patched conic ephemeris model) play a significantly greater role in the planetocentric cyclers. For these reasons, the transition to a high-fidelity force model is substantially more difficult for the planetocentric cyclers. To demonstrate the transition, Table 8 summarizes the results of optimized single cycles of four example cyclers in high-fidelity models using the patched conic ephemeris solutions as initial guesses.

Close approaches with flyby radii less than 200,000 km to all moons with gravitational parameters larger than 1 $\mathrm{km}^3/\mathrm{s}^2$ are reported in Table 8. Note that only one low-altitude targeted flyby of Enceladus or Europa results from the initial guess. However, several high-altitude serendipitous encounters with Enceladus occur in each of the cases a–c. In particular, note that case c includes an extra very-low-altitude Enceladus encounter with a flyby altitude of 4 km. The case a Titan–Enceladus cycler #183 includes one very-low-altitude (3 km) and two high-altitude Enceladus flybys, four medium-altitude

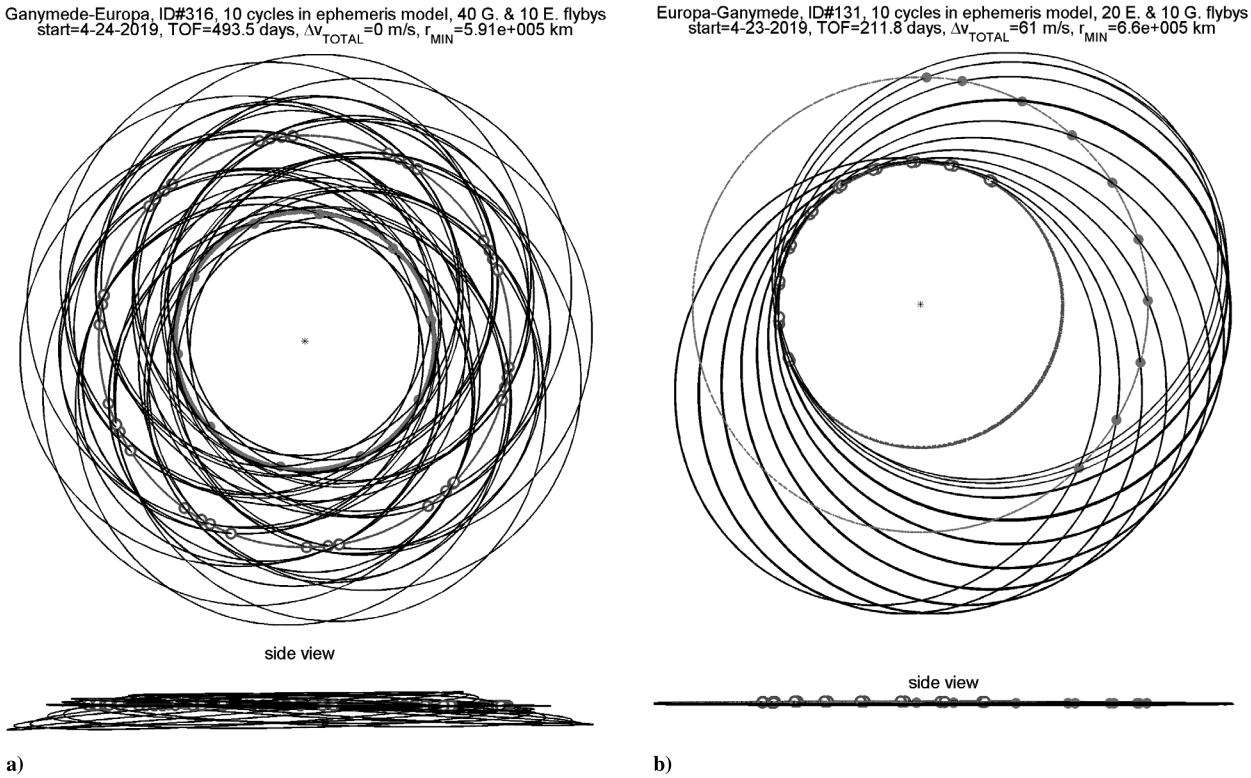

Fig. 9 Example Ganymede–Europa and Europa–Ganymede ephemeris patched conic cyclers.

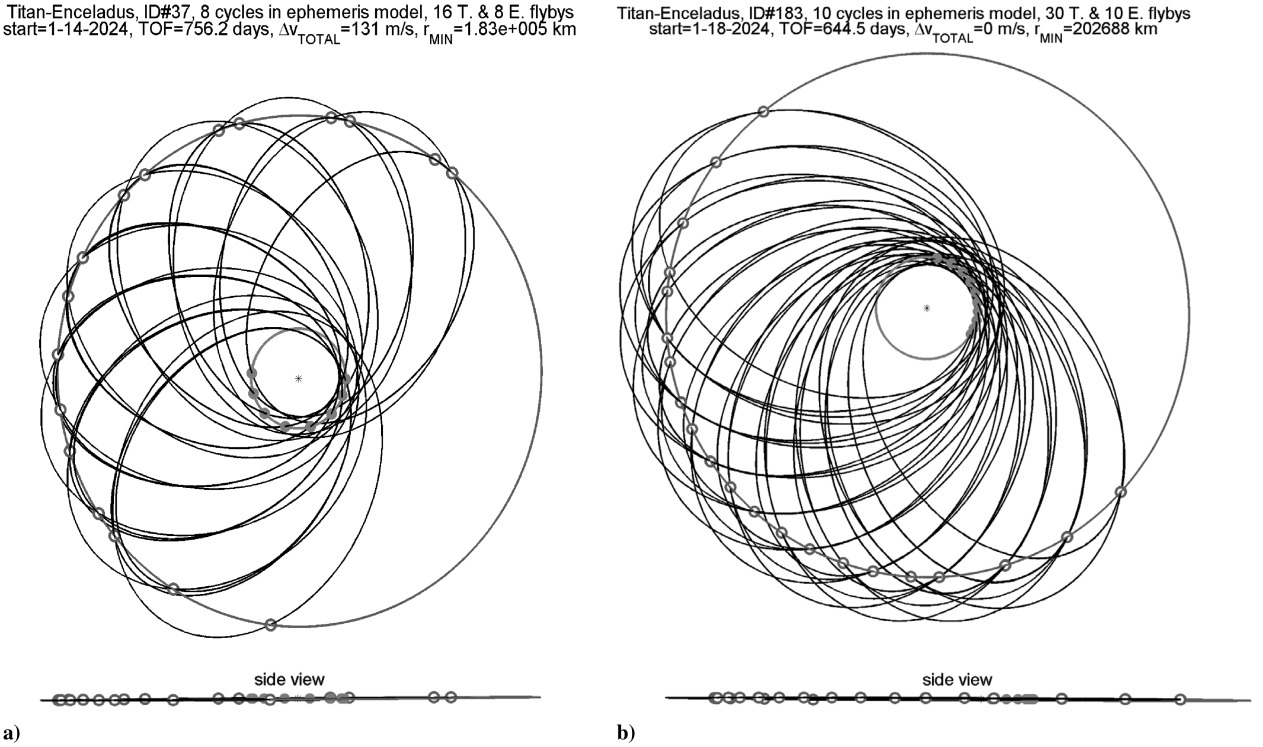

Fig. 10 Example low v_∞ Titan–Enceladus ephemeris patched conic cyclers, Part 1.

Titan encounters, and many untargeted moon encounters costing a total Δv of 32 m/s. The case b Titan–Enceladus cycler #235 includes six low-altitude Titan, one low-altitude Enceladus, six high-altitude Enceladus, and many untargeted moon encounters costing a total Δv of 63 m/s. Note that a second independently optimized cycle of Titan–Enceladus cycler #235 required a total Δv of 40 m/s. The case c Titan–Enceladus cycler #586 includes three medium-altitude Titan, two low-altitude Enceladus, four high-altitude Enceladus, and many untargeted moon encounters costing a total Δv of 11 m/s. Note that the v_∞ at Titan is ~5.75 km/s, making this example applicable for a Cassini extended mission. The case d Ganymede–Europa cycler #316 includes five targeted Ganymede, one targeted Europa, and no untargeted moon encounters costing a total Δv of 121 m/s. Although not documented in Table 8, a high-fidelity simulation of one cycle of the Europa–Ganymede cycler #131 costs a total Δv of 58 m/s and includes an extra close flyby of Europa.

As anticipated, the patched conic ephemeris solutions with the very high flyby radii are generally more difficult to converge to the

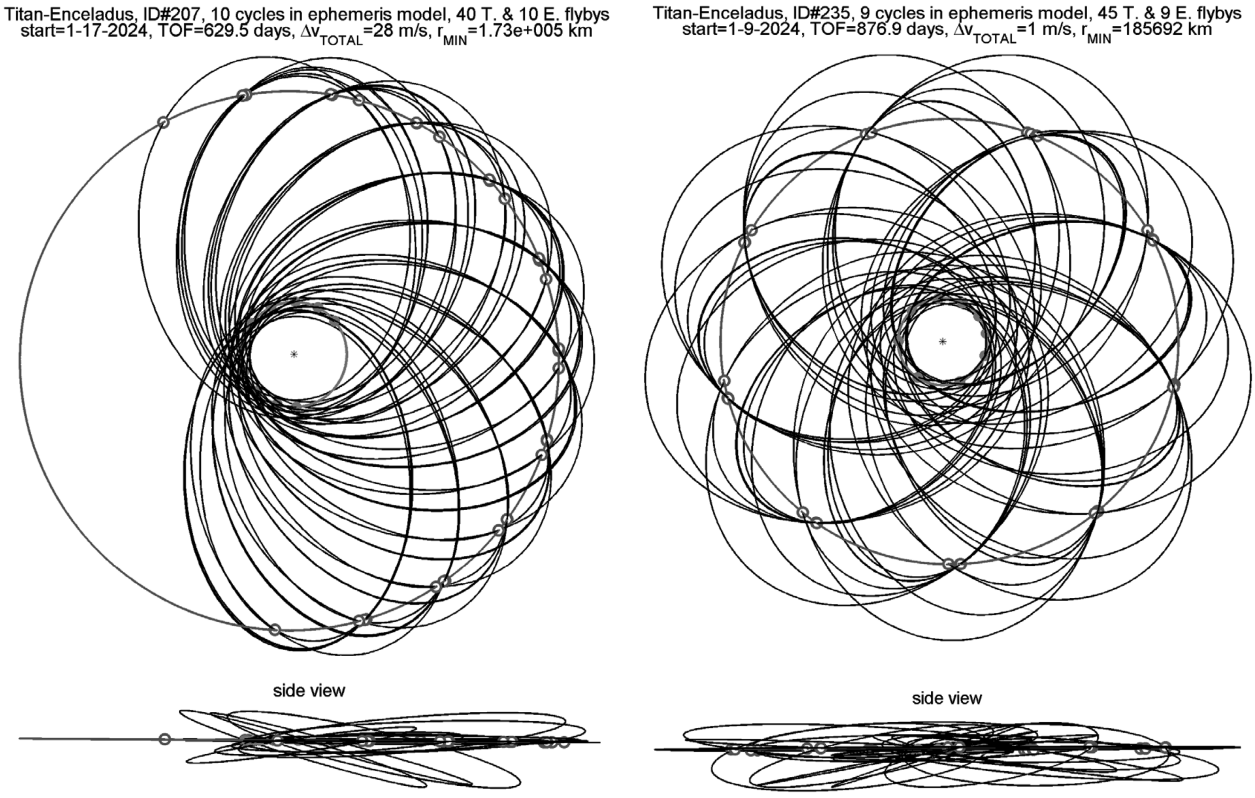

a) b)

Fig. 11 Example low v_∞ Titan–Enceladus ephemeris patched conic cyclers, Part 2.

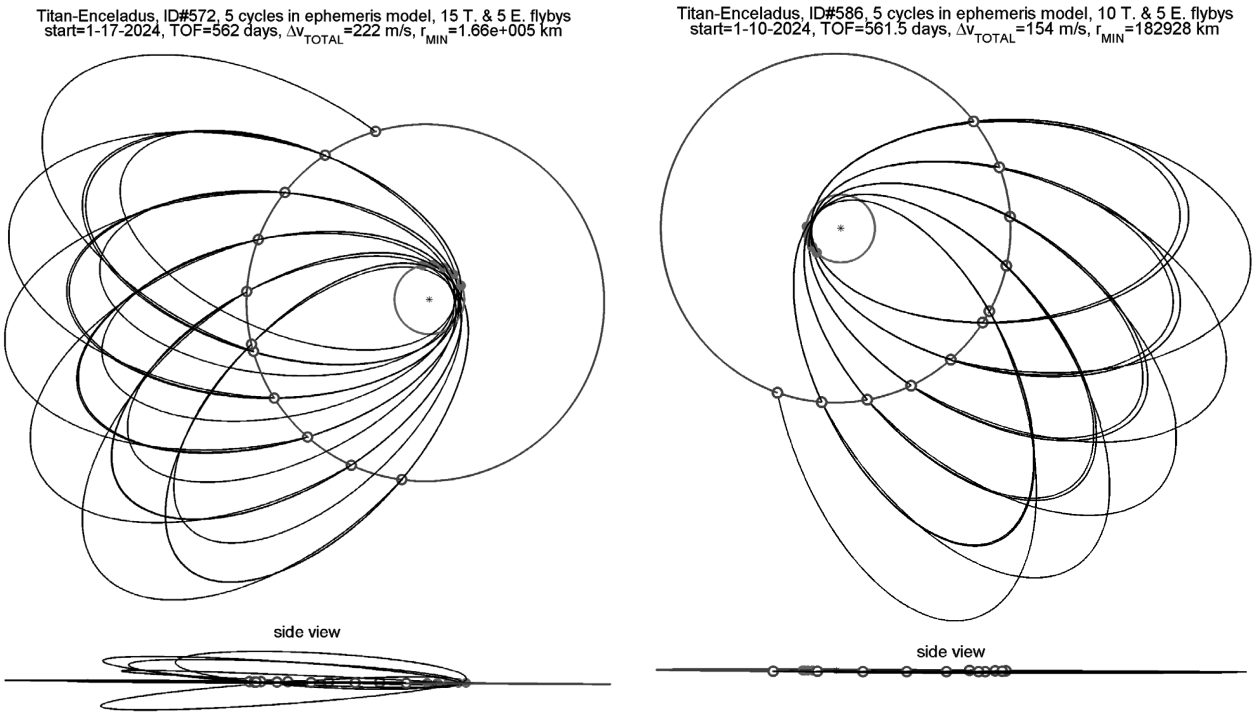

a) b)

Fig. 12 Example high v_∞ Titan–Enceladus ephemeris patched conic cyclers (applicable to Cassini extended missions).

low Δv solutions in the high-fidelity models because of the large violation of the zero radius sphere of influence assumption. Future work includes seeking methods to mitigate this effect, such as altering the constants in the lower-fidelity models to mimic the more realistic timing and geometry in the high-fidelity model. In addition, improved ideal model (circular–coplanar) cyclers could be sought by removing the massless assumption of the target body [18]. In particular, the Jovian system cyclers would benefit from such a change.

The design of high-fidelity moon tours is generally a time-consuming process involving an artistic combination of methods, software, and intuition. The examples included here are meant to

Table 7 Details[a] on the patched conic ephemeris Titan–Enceladus cycler #235 from Fig. 11b

Leg no.	Start (T or E)	TOF, day	v_∞, km/s	RA, deg	DEC, deg	Leg no.	Start (T or E)	TOF, day	v_∞, km/s	RA, deg	DEC, deg
1	T	14.187	3.103	105.17	−25.25	28	T	10.507	3.246	−43.35	15.75
2	T	19.570	3.145	170.61	0.81	29	E	5.444	5.951	−6.82	−3.17
3	T	31.891	3.115	137.84	−20.69	30	T	15.946	3.257	−32.21	29.65
4	T	10.459	3.114	153.69	−8.13	31	T	14.063	3.257	−51.66	18.92
5	E	5.489	5.506	−174.11	10.05	32	T	19.509	3.206	9.19	−10.24
6	T	15.945	3.120	155.95	−12.06	33	T	31.891	3.239	−23.19	11.67
7	T	14.118	3.120	146.02	−11.62	34	T	10.539	3.239	−8.05	−1.28
8	T	19.600	3.172	−152.35	18.14	35	E	5.403	6.901	26.67	−18.86
9	T	31.891	3.145	178.52	−6.37	36	T	15.945	3.229	3.55	12.02
10	T	10.458	3.145	−169.54	10.17	37	T	14.130	3.229	−15.92	2.62
11	E	5.494	4.499	−135.54	25.54	38	T	19.484	3.178	47.86	−24.19
12	T	15.945	3.162	−166.67	4.98	39	T	31.891	3.205	11.06	−5.46
13	T	14.051	3.162	−177.16	7.13	40	T	10.554	3.205	27.66	−17.78
14	T	19.607	3.200	−109.57	27.44	41	E	5.382	7.423	64.74	−27.85
15	T	31.891	3.187	−144.72	10.96	42	T	15.945	3.186	37.34	−3.58
16	T	10.481	3.187	−129.14	24.24	43	T	14.189	3.186	18.96	−14.66
17	E	5.473	4.185[b]	−90.73	28.61	44	T	19.483	3.158	91.48	−27.16
18	T	15.946	3.211	−129.89	43.74	45	T	31.891	3.164	50.27	−13.39
19	T	14.014	3.211	−137.83	22.79	46	T	10.540	3.164	68.81	−26.96
20	T	19.590	3.216	−65.03	23.05	47	E	5.394	7.380	107.11	−25.37
21	T	31.891	3.223	−104.96	24.03	48	T	15.945	3.142	71.05	−17.91
22	T	10.485	3.223	−84.26	26.48	49	T	14.212	3.142	58.94	−26.25
23	E	5.471	4.851	−43.15	15.31	50	T	19.510	3.150	132.82	−17.26
24	T	15.946	3.250	−77.08	42.78	51	T	31.891	3.133	90.55	−15.82
25	T	14.018	3.250	−93.47	27.51	52	T	10.506	3.133	112.37	−23.47
26	T	19.550	3.221	−26.26	7.91	53	E	5.428	6.740	147.10	−10.89
27	T	31.891	3.246	−56.82	33.89	54	T	15.945	3.110	111.26	−13.18

[a]The propagation is a zero radius sphere of influence patched conic and the ephemeris positions of the moons are relative to a fixed Saturn. Right ascension (RA) and declination (DEC) are expressed in the ecliptic J2000 frame. The start date is 8774.549 days after J2000 (10 Jan. 2024).
[b]For orbiting or landing at Enceladus, a mission designer should target the lowest $v\infty$ of all the Enceladus encounters. Note that the minimum possible in the ideal model is from the Hohmann transfer: Enceladus $v_\infty = 3.71$ km/s, Titan $v_\infty = 2.39$ km/s.

Table 8 Single cycles optimized in high-fidelity models[a,b,c]

Titan–Enceladus #183			Titan–Enceladus #235			Titan–Enceladus #586			Ganymede–Europa #316		
Encounter	t, day	Flyby alt., km or Δv	Encounter	t, day	Flyby alt., km or Δv	Encounter	t, day	Flyby alt., km or Δv	Encounter	t, day	Flyby alt., km or Δv
Titan	0.00	10,510	**Titan**	0.00	1858	**Titan**	0.00	4417	**Ganymede**	0.00	1224
Dione	7.13	2879	Δv	8.95	**1.1 m/s**	Tethys	1.51	11,656	Δv	8.78	**78.7 m/s**
Dione	7.36	79,911	Rhea	9.27	49,765	Enceladus	1.58	82,145	**Ganymede**	10.80	2094
Mimas	7.45	166,523	Δv	13.55	**13.2 m/s**	Dione	19.15	70,850	**Ganymede**	20.17	4778
Rhea	16.63	47,197	**Titan**	19.58	2040	Enceladus	19.33	154,979	Δv	23.31	**42.4 m/s**
Mimas	27.26	176,755	Dione	22.08	115,461	Rhea	19.99	578	**Europa**	27.72	495
Δv	27.29	**8.8 m/s**	Enceladus	22.30	145,151	Enceladus	37.13	180,599	**Ganymede**	39.99	8230
Enceladus	27.36	169,665	Tethys	22.32	91,913	Dione	54.75	58,404	**Ganymede**	49.35	1492
Rhea	27.72	7541	Δv	23.30	**7.5 m/s**	Enceladus	54.94	184,774			
Titan	34.36	3670	Rhea	33.38	70,927	Δv	54.98	**6.5 m/s**			
Δv	37.10	**1.4 m/s**	**Titan**	51.49	1000	Tethys	55.27	106,293			
Enceladus	37.18	151,288	Enceladus	54.19	172,350	**Enceladus**	72.92	912			
Mimas	44.96	129,365	**Enceladus**	61.92	3	Δv	73.08	**1.6 m/s**			
Enceladus	45.02	3	Mimas	62.00	145,679	Dione	90.97	182,699			
Mimas	45.12	87,092	Tethys	62.07	76,144	Δv	91.00	**3.2 m/s**			
Titan	50.27	9234	Mimas	62.24	155,684	Enceladus	91.16	4			
Rhea	52.45	113,199	Δv	63.55	**20.0 m/s**	Tethys	91.22	191,625			
Tethys	53.21	48,754	**Titan**	67.44	1801	**Titan**	92.81	4889			
Dione	61.52	148,847	Enceladus	70.13	114,438	**Titan**	112.30	5693			
Δv	61.90	**22.2 m/s**	Enceladus	70.39	165,493						
Titan	64.45	10,201	Δv	70.45	**21.1 m/s**						
			Hyperion	74.79	81,157						
			Mimas	78.17	62,970						
			Titan	83.39	999						
			Δv	94.70	**0.2 m/s**						
			Enceladus	94.78	93,155						
			Enceladus	95.03	127,658						
			Titan	97.47	2232						

[a]Begin date for the four cyclers is, respectively, 1 Feb. 2024 3:23:12; 24 Jan. 2024 3:59:16; 29 Jan. 2024 15:24:38; and 3 May 2019 12:17:26.
[b]Total Δv for the four cyclers is 32, 63, 11, and 121 m/s, respectively
[c]Bold encounters result from the ideal model cycler geometry, whereas the others are serendipitous and initially untargeted.

demonstrate the feasibility of realistic planetary moon cyclers. Detailed refinement of each reported sequence would likely lead to improved Δv costs. Further, it is emphasized that the boundary conditions on each sequence are heavily constrained so that the timing and geometry of the cycler is maintained. Relaxing these constraints is another source that can reduce Δv costs. As an example, by adding one extra Titan leg and reoptimizing the sequence presented in Table 8 (first column), the total Δv reduces from 32 to 17 m/s. This dramatic improvement is not indicative of all cases. However, large maneuvers near the end of a sequence can often be significantly reduced by including additional flybys. In general, patching together and optimizing multiple cycles, such as the 54 leg cycler illustrated in Table 7 and Fig. 11b, is beyond the scope of the software and intent of the present study. Future work includes automating methods to enable such multicycle optimization in the high-fidelity models. Furthermore, we note that the examples presented are representative of expected results, whereas high-fidelity optimization of each case presented in Table 4 is not currently practical.

Conclusions

Existing cycler search algorithms previously applied to the Earth–Mars case are generalized and improved for application to the planetary moon cycler problem. The short synodic periods of the planetary moon systems significantly widens the design space for finding useful cycler trajectories. As a result, the existence of hundreds of ideal model ballistic cyclers is demonstrated for the Galilean moon pairs at Jupiter and the Titan–Enceladus moon pair at Saturn, with repeat times ranging from $\sim$2 to $\sim$18 weeks. The complete database is archived and can be queried or sorted for quick assessment of the cycler architecture and preliminary guesses for future planetary moon mission and tour design applications.

For evaluation in a more realistic model, an improved homotopy method is implemented that seeks multiple cycles of ballistic solutions in a patched conic ephemeris model. Notably, many of the multicycle trajectories that include up to 54 flybys remain ballistic and several resulting examples are documented. As a feasibility demonstration, we optimize single cycles of four representative cyclers in a high-fidelity force model based on initial guesses from the patched conic ephemeris model. The preliminary analysis suggests that the high-fidelity force models often differ significantly from the zero radius sphere of influence patched conic ephemeris model for the planetary moon systems considered. However, for the Titan–Enceladus high-fidelity examples, we find that the Δv costs per flyby are similar in magnitude to Cassini, noting that the solutions are heavily epoch dependent and further refinement would likely improve the results. Future work is required to further assess the viability and strategies of designing realistic cyclers.

Special attention is paid to the Titan–Enceladus system because of the recent heightened science interest due to Cassini and the exceptional accuracy of the massless Enceladus assumption. Of the low-energy Titan–Enceladus cyclers, several are recommended as promising because of short periods, frequent encounters with both bodies, multiple degrees of freedom and flyby geometries at Titan, potential for full lighting conditions, and low approach velocities at Enceladus. The high-energy Titan–Enceladus cyclers are candidates for the Cassini extended missions, which undoubtedly will require frequent, low-cost encounters with Enceladus.

The generalized free-return cycler theory provides alternative and complementary methods to explore some of the highest priority celestial bodies according to the planetary science community, including Titan, Enceladus, and the Galilean moons at Jupiter. The repeat flybys of a cycler enable remote sensing surface science as well as in situ measurements of atmospheres, electromagnetic fields, and plumes. The planetary cycler trajectories can act as standalone flyby missions or as road maps of the trade space for the traditional planetary tour design problem. Furthermore, a cycler can provide invaluable reconnaissance and act as a telecommunications relay for surface landers, orbiters, or aerial vehicles. For a very low propellant cost and only a modest percentage increase in total mission duration, the cycler architecture is an attractive option for maximizing science for a variety of planetary moon missions.

Acknowledgments

The authors thank Kim Reh, Tom Spilker, Jim Cutts, and Brent Buffington for their interest and support. Part of this work was carried out at the Jet Propulsion Laboratory, California Institute of Technology, under a contract with NASA.

References

[1] Bagenal, F., Dowling, T. E., and McKinnon, W. B., *Jupiter: The Planet, Satellites and Magnetosphere*, Cambridge Univ. Press, Cambridge, England, U.K., 2004, pp. 281–306.

[2] Khurana, K. K., Kivelson, M. G., Stevenson, D. J., Schubert, G., Russel, C. T., Walker, R. J., and Polanskey, C., "Induced Magnetic Fields as Evidence for Subsurface Oceans in Europa and Callisto," *Nature (London)*, Vol. 395, Oct. 1998, pp. 777–780. doi:10.1038/27394.

[3] Hansen, C. J., Esposito, L., Stewart, A. I. F., Colwell, J., Hendrix, A., Pryor, W., Shemansky, D., and West, R., "Enceladus' Water Vapor Plume," *Science*, Vol. 311, No. 5766, March 2006, pp. 1422–1425. doi:10.1126/science.1121254.

[4] Porco, C. C., Helfenstein, P., Thomas, P. C., Ingersoll, A. P., Wisdom, J., West, R., Neukum, G., Denk, T., Wagner, R., Roatsch, T., Kieffer, S., Turtle, E., McEwen, A., Johnson, T. V., Rathbun, J., Veverka, J., Wilson, D., Perry, J., Spitale, J., Brahic, A., Burns, J. A., DelGenio, A. D., Dones, L., Murray, C. D., and Squyres, S., "Cassini Observes the Active South Pole of Enceladus," *Science*, Vol. 311, No. 5766, March 2006, pp. 1393–1401. doi:10.1126/science.1123013.

[5] Rall, C. S., "Freefall Periodic Orbits Connecting Earth and Mars," Ph.D. Thesis, Dept. of Aeronautics and Astronautics, Massachusetts Inst. of Technology, Cambridge, MA, Oct. 1969.

[6] Hollister, W. M., "Periodic Orbits for Interplanetary Flight," *Journal of Spacecraft and Rockets*, Vol. 6, No. 4, 1969, pp. 366–369. doi:10.2514/3.29664

[7] Byrnes, D. V., Longuski, J. M., and Aldrin, B."Cycler Orbit Between Earth and Mars," *Journal of Spacecraft and Rockets*, Vol. 30, No. 3, May–June 1993, pp. 334–336. doi:10.2514/3.25519

[8] Nock, T., Duke, M., King, R., Jacobs, M., Johnson, L., McRonald, A., Penzo, P., Rauwolf, J., and Wyszowski, C., "An Interplanetary Rapid Transit System Between Earth and Mars," *Expanding the Frontiers of Space; Space Technology and Applications International Forum, STAIF 2003*, edited by M. S. El-Genk, American Inst. of Physics, Melville, NY, 2003, pp. 1074–1086.

[9] Russell, R. P., and Ocampo, C. A., "Systematic Method for Constructing Earth–Mars Cyclers Using Free-Return Trajectories," *Journal of Guidance, Control, and Dynamics*, Vol. 27, No. 3, 2004, pp. 321–335. doi:10.2514/1.1011

[10] Russell, R. P., and Ocampo, C. A., "Geometric Analysis of Free-Return Trajectories Following a Gravity-Assisted Flyby," *Journal of Spacecraft and Rockets*, Vol. 42, No. 1, 2005, pp. 138–151. doi:10.2514/1.5571

[11] Russell, R. P., and Ocampo, C. A., "Global Search for Idealized Free-Return Earth–Mars Cyclers," *Journal of Guidance, Control, and Dynamics*, Vol. 28, No. 2, 2005, pp. 194–208. doi:10.2514/1.8696

[12] McConaghy, T. T., Russell, R. P., and Longuski, J. M., "Towards a Standard Nomenclature for Earth–Mars Cycler Trajectories," *Journal of Spacecraft and Rockets*, Vol. 42, No. 4, 2005, pp. 694–698. doi:10.2514/1.8123

[13] Russell, R. P., and Ocampo, C. A., "Optimization of a Broad Class of Ephemeris Model Earth–Mars Cyclers," *Journal of Guidance, Control, and Dynamics*, Vol. 29, No. 2, 2006, pp. 354–367. doi:10.2514/1.13652

[14] McConaghy, T. T., Yam, C. H., Landau, D. F., and Longuski, J. M., "Two-Synodic-Period Earth–Mars Cyclers with Intermediate Earth Encounter," American Astronautical Society Paper 03-509, Aug. 2003.

[15] Byrnes, D. V., McConaghy, T. T., and Longuski, J. M., "Analysis of Various Two Synodic Period Earth–Mars Cycler Trajectories," AIAA Paper 2002-4423, Aug. 2002.

[16] Niehoff, J., "Pathways to Mars: New Trajectory Opportunities," American Astronautical Society Paper 86-172, July 1986.

[17] Turner, A., "Low Road to Mars: The Venus-Mars Cycler," American Astronautical Society Paper 07-175, Jan. 2007.
[18] Pisarevsky, D. M., Kogan, A., and Guelman, M., "Interplanetary Periodic Trajectories in Two-Planet Systems," *Journal of Guidance, Control, and Dynamics*, Vol. 31, No. 3, 2008, pp. 729–739. doi:10.2514/1.30046
[19] Chen, K., McConaghy, T., Okutsu, M., and Longuski, J., "A Low-Thrust Version of the Aldrin Cycler," AIAA Paper 2002-4421, Aug. 2002.
[20] Landau, D. F., and Longuski, J. M., "Guidance Strategy for Hyperbolic Rendezvous," AIAA Paper 2006-6299, Aug. 2006.
[21] Whiffen, G. J., and Sims, J. A., "Application of the SDC Optimal Control Algorithm to Low-Thrust Escape and Capture Trajectory Optimization," *AAS/AIAA Space Flight Mechanics Meeting*, American Astronautical Society Paper 02-208, 2002.
[22] Strange, N. J., and Sims, J. A., "Methods for the Design of V-Infinity Leveraging Maneuvers," American Astronautical Society Paper 01-437, Aug. 2001.
[23] Prussing, J. E., and Conway, B. A., *Orbital Mechanics*, Oxford Univ. Press, New York, 1993, pp. 63–80.
[24] Prussing, J. E., "A Class of Optimal Two-Impulse Rendezvous Using Multiple-Revolution Lambert Solutions," *Journal of the Astronautical Sciences*, Vol. 48, Nos. 2–3, April–Sept. 2000, pp. 131–148.
[25] Shen, H., and Tsiotras, P., "Using Battin's Method to Obtain Multiple-Revolution Lambert's Solutions," American Astronautical Society Paper 03-568, Aug. 2003.
[26] Russell, R. P., and Strange, N. J., "Planetary Moon Cycler Trajectories," *AAS/AIAA Space Flight Mechanics Meeting*, American Astronautical Society Paper 07-118, Jan. 2006.
[27] Seidelmann, P. K., Abalakin, V. K., Bursa, M., Davies, M. E., de Bergh, C., Lieske, J. H., Oberst, J., Simon, J. L., Standish, E. M., Stooke, P., and Thomas, P. C., "Report of the IAU/IAG Working Group on Cartographic Coordinates and Rotational Elements of the Planets and Satellites: 2000," *Celestial Mechanics and Dynamical Astronomy*, Vol. 82, No. 1, 2002, pp. 83–111. doi:10.1023/A:1013939327465
[28] Wiesel, W. E., *Spaceflight Dynamics*, McGraw–Hill, Boston, 1997, p. 300.